Grid-Forming Control VSC-Based Including Current Limitation and Re-synchronization Functions to Deal with Symmetrical and Asymmetrical Faults

Taoufik Qoria, Xiongfei Wang, Riad Kadri

***Abstract*—Grid-forming converters operate as voltage sources behind impedance. This property makes them robust against Short-Circuit Ratio (SCR) variation, but vulnerable against large grid disturbances. As a precaution, grid-forming converters have to embed adequate control algorithms to ensure a stable system operation under various grid conditions, to deal with excessive overloadings mainly caused by faults, and to guarantee a stable re-synchronization after fault clearance. These expectations have been met in previous works considering balanced conditions. Nevertheless, the extension of the grid-forming control to deal with unbalanced grid conditions considering current limitation and angular stability is a point rarely discussed in the literature. To fill this research gap, this paper proposes an Extended Power Synchronization Method (EPSM) that allows the system to operate under balanced and unbalanced grid conditions while meeting the Fault Ride-Through requirements (FRT). The proposed method is a direct voltage control-based, which embeds a threshold current control loop, which is enabled only when a fault is detected. Additionally, the control is equipped with an algorithm that modifies the active power control during faults to aid the power converter to be remain synchronized after fault clearance. The effectiveness of the proposed control has been demonstrated through time-domain simulations.**

***Keywords*—Grid-forming, Unbalanced Grid Voltage, Power Synchronization, Fault Ride-Through, Current Limitation.**

I. Introduction

THE modern power systems are undergoing significant changes due to the everlasting integration of Intermittent Renewable Energy Sources (IRES) and the High Voltage Direct Current (HVDC) links. These factors result in a significant increase of power electronic converters in the power systems. Nowadays, power converters have the main function of injecting the power into the main grid, while relying on synchronous machines that ensure all system needs. This control mode known as "Grid-following" [1] has several limitations reported in the literature starting from its inability to operate in a standalone mode and its negative side effect on the total system inertia [2], which call into question the reliability of the future electrical system dominated by power electronic converters. To tackle these challenges, the grid-forming capability appears as a promising solution since it allows the converter to operate as a voltage source, and to mimic some characteristics of synchronous generators (i.e., emulation of the swing equation) [3], [4], [5], [6]. Nevertheless, due to the voltage source behavior of the grid-forming converters, the overcurrent protection remains their ultimate challenge i.e., semiconductor components-based power converters have a limited overloading capability [7] and their over-sizing is a cost non-effective and non-attractive solution. Hence, the major efforts on the protection aspects have to be done via the software. In this context, two main control techniques have already been proposed in the literature to face overcurrent issues. The first technique consists in saturating the current reference (CSA) [8], [9], [10], [11]. The second one is based on a variable virtual impedance (VI), which artificially increases the output impedance when the current exceeds its nominal value [12], [13], [14], [15].

In prior works, the authors were mainly focused on balanced conditions with and without faults. While, few research have covered the unbalanced system operation under normal and particularly in abnormal conditions [8], [11], [17], [18]. Authors in [8], [11] have used current saturation techniques for grid-forming converters to deal with unbalanced faults considering Two-Level and Modular Multilevel Converters (MMC) topologies, respectively. Nonetheless, the aforementioned works were limited to the standalone operation mode, in which the converter frequency is constant and the angular stability aspect is not a concern. Therefore, these solutions are not adapted for the grid-connected mode, in which the converter re-synchronization during the post-fault phase is of a high interest. In [17], the authors extend the virtual impedance to face unbalanced grid faults. The complexity of this method relies on its dependency on the grid output impedance in unbalanced situations. In [18], the authors have implemented a current limitation technique in the (abc) frame. The solution shows its effectiveness to deal with unbalanced faults in steady-state. Nevertheless, the current dynamics in the transient still need to be improved i.e., the authors have used a KALMAN filter to estimate the currents, which induces a time delay in the control and thereby increases its complexity. Additionally, the post-fault phase after fault clearance has not been shown and discussed. In a recent work [19], a current limitation based on the current reference saturation and the virtual impedance has been proposed. The control has been designed in the stationary-frame ($\alpha\beta$)

This work was supported by Maschinenfabrik Reinhausen Gmbh.

Q. Taoufik is with Maschinenfabrik Reinhausen Gmbh, Regenesburg, Germany, e-mail: T.qoria@reinhausen.com.

Xiongfei Wang is with Aalborg Universitet Teknisk-Naturvidenskabelige Fakultet, Department of Energy Technology.

Riad Kadri is with Univ. Lille, Arts et Metiers Institute of Technology, Centrale Lille, Yncrea Hauts-de-France, ULR 2697 Laboratoire d'Electrotechnique et d'Electronique de Puissance, F-59000 Lille, France

Paper submitted to the International Conference on Power Systems Transients (IPST2023) in Thessaloniki, Greece, June 12-15, 2023.

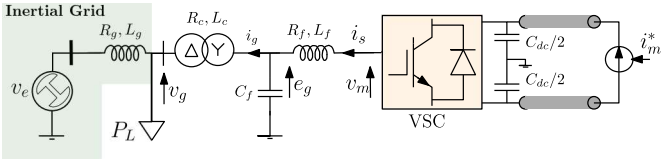

Fig. 1. Studied System

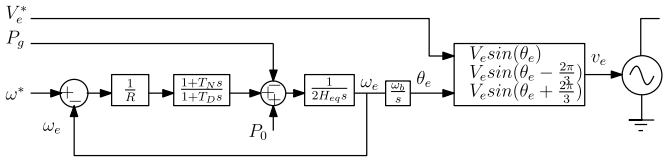

Fig. 2. Inertial AC grid, H_{eq} = 5s, T_1 = 1s, T_2 = 2s, R = 0.04 p.u

considering cascaded Proportional-Resonant (PR) controllers. Referring to [2], the cascaded control structure requires tuning efforts to guarantee a stable system with the desired performances. In the other hand, although the obtained results show satisfactory performances from a current limitation point of view, the angular stability aspect was missing in this work.

Based on the state-of-the-art, the novelty of this paper consists in proposing an Extended Power Synchronization Method (EPSM) to operate under balanced and unbalanced grid conditions. The particularity of this control method lies in the simplicity of its design and implementation. The EPSM operates as a direct voltage control when no fault is detected. Once a fault occurs, the control switches naturally to the current control mode to prevent overcurrent. Additionally, the control adopts a re-synchronization aid function to limit the frequency variation during the fault phase and to allow the converter remaining connected to the grid during the post-fault phase. The effectiveness of the proposed solution is demonstrated through time-domain simulations performed in MATLAB/SimPowerSystem.

The reminder of this paper is organized as follows. In section II, the studied system is modeled considering the positive and negative sequences in $d-q$ frame. Then, the proposed grid-forming EPSM method is presented and discussed in section III. Finally, section IV concludes the paper.

II. System Modeling

The power model of the studied system is presented in Fig. 1. The VSC is supplied by a controllable current source i_m^* that emulates the other side of a point-to-point HVDC link. The input i_m^* is given by a DC voltage regulator given in the appendix. From the AC side, the VSC is connected to the grid through an LC filter and a $(\mathbf{Y_g}/\mathbf{\Delta})$ transformer. The AC grid is modeled by a power load P_L and an equivalent inertial AC voltage source v_e in series with its equivalent impedance R_g,L_g. The inertial source includes the frequency governor, a lead-lag function to emulate the dynamic of the turbine, and the swing equation [26]. The illustration of the inertial AC source is given in Fig. 2.

The dynamic equations of the system in $(\alpha\beta)$-domain are formulated as follows:

$$\dot{i_{s_{\alpha\beta}}} = \frac{1}{L_f}\left(v_{m_{\alpha\beta}} - e_{g_{\alpha\beta}}\right) - \frac{R_f}{L_f} i_{s_{\alpha\beta}} \tag{1}$$

$$\dot{e_{g_{\alpha\beta}}} = \frac{1}{C_f}\left(i_{s_{\alpha\beta}} - i_{g_{\alpha\beta}}\right) \tag{2}$$

$$\dot{i_{g_{\alpha\beta}}} = \frac{1}{L_c}\left(e_{g_{\alpha\beta}} - v_{g_{\alpha\beta}}\right) - \frac{R_c}{L_c} i_{g_{\alpha\beta}} \tag{3}$$

The system state variables are the VSC output current i_s flowing through the filter L_f, the AC voltage e_g across the capacitor filter C_f and the grid current i_g flowing through the transformer impedance L_c. The modulated and the grid voltages are denoted by v_m and v_g, respectively.

To control the system in unbalanced conditions, the electrical variables are decomposed into positive and negative sequences using the Fortescue-based matrix [20]. In the practice, Low-Pass and High-Pass filters are used to remove the second order harmonic 2ω and to shift the signal x by 90° (see Fig. 3).

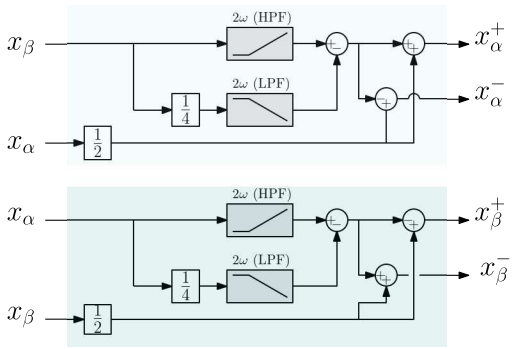

Fig. 3. Sequence extraction using Fortescue Matrix-Based Filter

By multiplying the output signals $x_{\alpha\beta}^{\pm}$ with the rotational matrices in (4)-(5), $d-q$ signals can be obtained, i.e., the per-unit system equations in (1)-(3) are expressed in the SRF as in (6)-(8).

$$R^{+}(\theta_m) = \begin{bmatrix} \cos(\theta_m) & \sin(\theta_m) \\ -\sin(\theta_m) & \cos(\theta_m) \end{bmatrix} \tag{4}$$

$$R^{-}(\theta_m^{-}) = \begin{bmatrix} \cos(\theta_m) & -\sin(\theta_m) \\ \sin(\theta_m) & \cos(\theta_m) \end{bmatrix} \tag{5}$$

$$si_{s_{dq}}^{\pm} = \frac{\omega_b}{L_f}\left(v_{m_{dq}}^{\pm} - e_{g_{dq}}^{\pm}\right) - \left(\frac{R_f}{L_f} i_{s_{dq}}^{\pm} \pm \omega_m i_{s_{dq}}^{\pm}\right)\omega_b \tag{6}$$

$$se_{g_{dq}}^{\pm} = \frac{\omega_b}{C_f}\left(i_{s_{dq}}^{\pm} - i_{g_{dq}}^{\pm}\right) \mp \omega_b \omega_m e_{g_{fq}}^{\pm} \tag{7}$$

$$si_{g_{dq}}^{\pm} = \frac{\omega_b}{L_c}\left(e_{g_{dq}}^{\pm} - v_{g_{dq}}^{\pm}\right) - \left(\frac{R_c}{L_c} i_{g_{dq}}^{\pm} \pm \omega_m i_{g_{dq}}^{\pm}\right)\omega_b \tag{8}$$

θ_m is the time-domain angle generated by the power control detailed in the next section. ω_b denotes the base system frequency in rad/s.

The instantaneous active and reactive power are given by (9) and (10), whereas P_{c_2}, P_{s_2}, Q_{c_2}, and Q_{s_2} are the second harmonic components resulted from the AC voltage unbalance.

$$P(t) = P_0 + P_{c_2}\cos(2\omega t) + P_{s_2}\sin(2\omega t) \tag{9}$$

$$Q(t) = Q_0 + Q_{c_2}\cos(2\omega t) + Q_{s_2}\sin(2\omega t) \tag{10}$$

III. Extended Grid-forming Power Synchronization Method

The Power Synchronization Method (PSM) is a direct AC voltage grid-forming control, which can switch to the current control mode only when the maximum allowable current is crossed. This method has been initially proposed in [16], but it was limited to symmetrical grid conditions. In this paper, the aforementioned method is extended to deal also with unbalanced grid conditions. Moreover, it includes different features that enhance the system stability and dynamics (i.e., Transient Virtual Resistance, LCL Active damping and a post-fault re-synchronization function). Each function is detailed in the following section.

A. Active Power Controller

The outer active power controller illustrated in Fig. 4 a is Lead-Lag filter-based power droop control [26].

$$\omega_m = \frac{m_p}{1+T_d s}\left[P^* - P^+\left(\frac{1+T_1 s}{1+T_2 s}\right)\right] + \omega_0 \tag{11}$$

$$\theta_m = \omega_m \omega_b / s \tag{12}$$

ω_0, T_d, m_p, T_1, T_2, P^* and P^+ denote the frequency setpoint in p.u, the Low-Pass-filter (LPF) time constant used to adapt the inertia constant, the droop gain, the lead-lag time constants, the active power setpoint and the positive sequence of the active power given in (13), respectively. Note that the lead-lag filter added to the droop control aims to damp the active power response, when the inertia constant $H = T_d/2m_p$ is set to H $\geq$ 1s. The tuning method of the Lead-lag filter is given in [26].

$$P^+ = V_{g_d}^+ I_{g_d}^+ + V_{g_q}^+ I_{g_q}^+ \tag{13}$$

B. Alternating-Voltage and Reactive Power Controllers

The VSC is a natural voltage source that could be directly driven by a set of AC voltage reference. Nevertheless, for a classical Two-Level VSC, the voltage is mainly controlled at the capacitor level, which is used to attenuate the THD_v of the modulated stage. The Alternating-Voltage Controller (AVC) is given by:

$$v_{m_d}^{*+} = \frac{k_{i_v}}{s}\left(E_g^{*+} - E_g^{f+}\right) + E_g^{*+} \tag{14}$$

$$v_{m_q}^{*+} = 0 \ \textbf{p.u} \tag{15}$$

E_g^{f+} and E_g^{*+} are the filtered measured AC voltage magnitude and the reference AC voltage magnitude, respectively. k_{i_v} is the integral voltage controller gain. The AC voltage magnitude E_g^{f+} is filtered using a first order LPF with ω_{ff} =2000 rad/s. The negative sequence of the AC voltage is set to zero.

$$v_{m_d}^{*-} = 0 \ \textbf{p.u}, \ \ v_{m_q}^{*-} = 0 \ \textbf{p.u} \tag{16}$$

If a reactive power compensation is needed, the output of the reactive power control given in (17) can be added to the AVC reference while being limited to $[\Delta E_{g_{min}}, \Delta E_{g_{max}}]$. The goal is to keep the grid voltage variations in the interval $\pm 10\%$ requested by the grid code.

$$\Delta V_{m_Q}^{*+} = \left[Q^* - Q^+\left(\frac{1}{1+T_Q s}\right)\right] n_q \tag{17}$$

In (17), Q^+, Q^*, n_q and T_Q denote the positive sequence of the reactive power given in (18), the reactive power reference setpoint, the reactive droop gain and the reactive power LPF time constant, respectively.

$$Q^+ = -V_{g_d}^+ I_{g_q}^+ + V_{g_q}^+ I_{g_d}^+ \tag{18}$$

The AVC and the reactive power blocks are shown in Fig. 5.

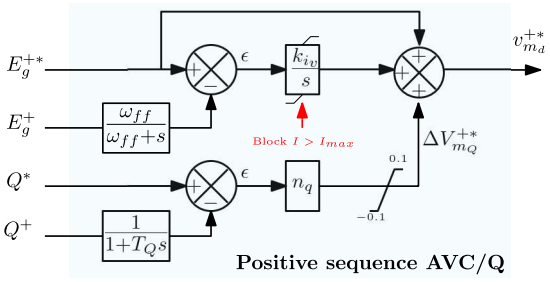

Fig. 5. Extended AVC and Reactive Power Control blocks

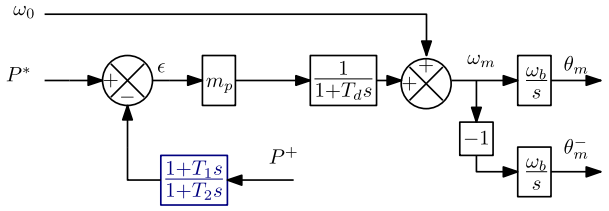

Fig. 4. Extended Lead-Lag filter-based droop control

C. Transient Virtual Resistor (TVR)

During transients, maintaining a constant voltage would induce synchronous oscillations due to the undamped line dynamics (X $\gg$ R) [2], especially in case of a connection to a stiff grid. These oscillations may result in an unstable system operation in case of fast active power response ($T_R^{5\%} \leq$ 100ms) [2]. To avoid such a consequence, a TVR should be adopted in the control to damp the grid current dynamics. As for the reactive power, the output voltages generated by the TVR $\delta v_{R_{dq}}^{\pm}$ should be added to the output voltages of the AVC. The TVR expression is given in the following line:

$$\delta v_{R_{dq}}^{\pm} = R_V\left(\frac{s}{\omega_f + s}\right) i_{g_{dq}}^{\pm} \tag{19}$$

R_v is the virtual resistor. ω_f is the cut-off frequency of the high-pass filter.

D. LCL Resonance damping

To avoid particular resonance linked to the LCL filter, which may be excited by fast transients, an active damping control has to be implemented. The active damping control in (20) acts as a physical resistor in series with the filter capacitor C_f, but only in the transient. It is given by the following equation:

$$\delta v_{LCL_{dq}}^{\pm} = \frac{R_{LCL_D} s}{\omega_R + s}\left(i_{s_d}^{\pm} - i_{g_d}^{\pm}\right) \tag{20}$$

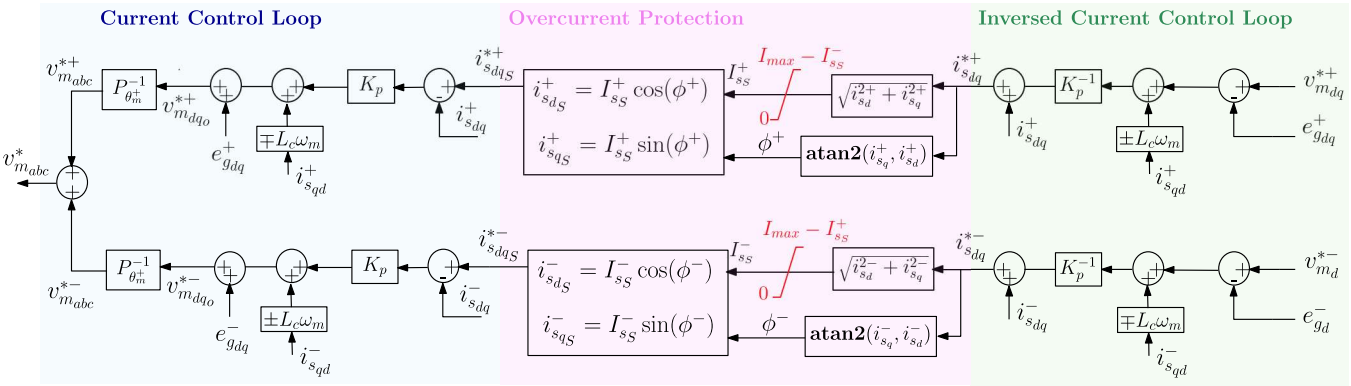

Fig. 6. Threshold Current Control Loops embedding the overcurrent protection function

The output voltages generated by the LCL active damping should be subtracted from the output voltages of the AVC.

E. Threshold-Current Control Loop

The control structure of the Threshold Current Control Loop (TCCL) is given in Fig. 6. The idea behind the TCCL is to generate $d-q$ current references from the functions (23)-(24) and their inverted ones in (21)-(22) for both positive and negative sequences. In this way, if the generated current reference $i^{*\pm}_{s_{dq}}$ did not reach its maximum value I_{max}, the functions (21) and (22) compensate (23) and (24), respectively. Hence, the input voltage reference $v^{*\pm}_{m_{dq}}$ will be equal to the output voltage $v^{*\pm}_{m_{dqo}}$, i.e., only the voltage control in Fig. 5 is interfering with the system. Once the maximum current I_{max} is exceeded because of a fault, a current saturation developed in section III.F is applied on $i^{*\pm}_{s_{dq}}$ to limit the current $i^{*\pm}_{s_{dq_S}}$. In this case, the system switches naturally to the current control mode. When the fault is cleared, the grid voltages $v^{\pm}_{g}$ are recovered leading to a natural switching of the control from the current mode to the direct voltage control mode where again $v^{*\pm}_{m_{dq}} = v^{*\pm}_{m_{dq_o}}$.
To achieve a perfect compensation between (21),(23) and (22),(24) in normal conditions, the choice of the controller C(s) is important: The controller should compulsory be proportional C(s) = K_p in order to be able to invert the control.

$$i^{+}_{s_{dq}} = i^{*^{+}}_{s_{dq}} - \left(v^{*^{+}}_{m_{dq}} \mp L_f\omega_m i^{+}_{s_{dq}} - e^{+}_{g_{dq}}\right) C(s)^{-1} \quad (21)$$

$$i^{-}_{s_{dq}} = i^{*^{-}}_{s_{dq}} - \left(v^{*^{-}}_{m_{dq}} \pm L_f\omega_m i^{-}_{s_{dq}} - e^{-}_{g_{dq}}\right) C(s)^{-1} \quad (22)$$

$$v^{*^{+}}_{m_{dq_o}} = \left(i^{*^{+}}_{s_{dq}} - i^{+}_{s_{dq}}\right) C(s) \pm L_f\omega_m i^{+}_{s_{dq}} + e^{+}_{g_{dq}} \quad (23)$$

$$v^{*^{-}}_{m_{dq_o}} = \left(i^{*^{-}}_{s_{dq}} - i^{-}_{s_{dq}}\right) C(s) \mp L_f\omega_m i^{-}_{s_{dq}} + e^{-}_{g_{dq}} \quad (24)$$

Assuming that the current saturation mode is enabled, the threshold current loop is activated (i.e., the VSC is controlled as a current injector). The closed-loop transfer function of the current loop is expressed as

$$\frac{i^{\pm}_{s_{dq}}}{i^{\pm *}_{s_{dqS}}} = \frac{1}{1+\tau_{des}s} \quad (25)$$

with $\tau_{des} = L_f/(\omega_b K_p)$. Based on the desired time response and acceptable steady state error, the gain K_p is chosen.

F. Current Limitation Technique

In faulty conditions, the current in each phase should not exceed the maximum allowable value I_{max} in steady-state:

$$I_{max} = \hat{I_s}^{+} + \hat{I_s}^{-} \quad (26)$$

$\hat{I}_s$ is the peak current value.
The proposed overcurrent protection algorithm embedded in Fig. 6 consists in limiting the positive and negative components in polar coordinates separately as given in (27).

$$\begin{cases} i^{\pm *}_{s_{dqS}} = i^{\pm *}_{s_{dq}} & \textbf{If} \quad I^{\pm}_{s} < I^{\pm}_{\max} \\ i^{\pm *}_{s_{dS}} = I^{\pm}_{\max}\cos\left[\mathbf{atan2}\left(\frac{\mathbf{i^{\pm *}_{sq}}}{\mathbf{i^{\pm *}_{sd}}}\right)\right] & \textbf{If} \quad I^{\pm}_{s} \geq I^{\pm}_{\max} \\ i^{\pm *}_{s_{qS}} = I^{+}_{\max}\sin\left[\mathbf{atan2}\left(\frac{\mathbf{i^{\pm *}_{sq}}}{\mathbf{i^{\pm *}_{sd}}}\right)\right] & \textbf{If} \quad I^{\pm}_{s} \geq I^{\pm}_{\max} \end{cases} \quad (27)$$

The positive and negative maximum allowable currents I^{+}_{max}, I^{-}_{max} are defined in such a way to respect (26). Depending on the fault type, the positive and negative current limits can not be reached simultaneously, e.g., in case of a three-phase bolted fault, only the positive sequence current is increasing, while the negative sequence current remain null. Therefore, I^{-}_{max} and I^{+}_{max} should be dependent and vary with respect to each other. In this context, (28) is adopted to limit the current without given any priority to one sequence over the other. The injected current will be defined by the type of fault and the inverted current control parameters.

$$\begin{cases} I^{-}_{max} = I_{max} - \sqrt{i^{2+}_{s_{dS}} + i^{2+}_{s_{qS}}} \\ I^{+}_{max} = I_{max} - \sqrt{i^{2-}_{s_{dS}} + i^{2-}_{s_{qS}}} \end{cases} \quad (28)$$

When the current is limited, the control switches from the voltage control mode to the current control mode. As a consequence, the AVC integrator induces a divergent output signal that may lead to the system instability. To avoid that, a voltage anti-windup is used i.e., once the current is limited, the control gain k_{i_v} is set to zero.

G. Transient Stability Enhancement

The transient instability occurs when no dedicated control algorithm is implemented to limit the frequency and the angle derivations during large disturbances. Referring to the analysis and the solution reported in [13], [21], [22], [23], [24], [25]

for balanced faults, the reduction of the active power during faults increases the critical clearing time and results in a higher transient stability margin. These analyzes remain effective under unbalanced conditions as long as the power angle is generated from the positive sequence of the active power as done in this paper. Indeed, when a fault occurs, (e.g., three-phase fault), the active power drops, while the power reference remains unchanged. This power mismatch engenders a frequency deviation, and thereby angle divergence. To avoid such a problem, the power reference has to be adapted naturally during faults in order to prevent the frequency from large deviations. The idea in this paper is to use the difference between the positive sequence of the AC voltage references $\lambda = \left(V_m^* - V_{m_0}^*\right)$ as adaptor for the active power reference: when no fault is present λ will always be equal to zero and hence, the adaptive power controller will be the same as the power controller in Fig. 4. When a fault occurs, $V_{m_0}^*$ will be reduced to limit the current to I_{max}. The obtained value of λ will be deduced from the power reference during the fault phase in order to limit the deviation of the frequency, and consequently increasing the transient stability margin. The proposed solution is given in (29) and illustrated in Fig. 7.

$$P_n^* = P^* - \underbrace{\left(V_m^* - V_{m_0}^*\right)}_{\lambda} \tag{29}$$

H. Validation and Test Cases

In this section, different events are applied to verify the control robustness against different transient scenarios that may occur in the transmission power systems. These scenarios are performed in the grid-connected mode. The system and control parameters are listed in Table I.

1) Short-Circuit Ratio (SCR) Variation: Illustrative simulations are performed in this subsection considering the grid case in Fig. 8. This test case is a grid impedance-switching scenario. The grid frequency is assumed to be fixed for this test ($\omega_e = 1$ p.u). When both impedances (X_{g_1}, R_{g_1} and X_{g_2}, R_{g_2}) are connected, the SCR = 3 (strong grid). When X_{g_2}, R_{g_2} is disconnected, the SCR decreases to 1.3 (very weak grid) and vice-versa. The corresponding values of these impedances are given in Table I. In Fig. 9, P^* is set to 0.8 p.u and only the line R_{g_1}, X_{g_1} is initially connected. At $t = 3.5$s the impedance X_{g_2}, R_{g_2} is connected. This event engenders a significant positive phase-shift of +0.436rad leading to a violent current transient. Thanks to the TCCL, the current has been accurately limited to its defined maximum value I_{max}.

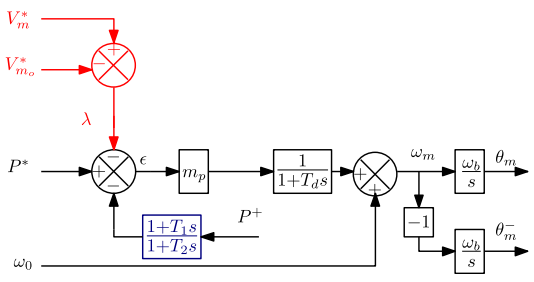

Fig. 7. Adaptive Extended Lead-Lag filter-based droop control

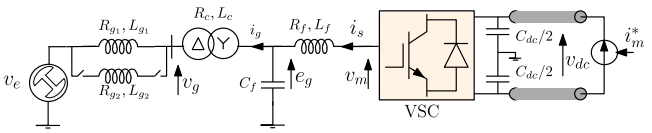

Fig. 8. Grid case for transient SCR variation

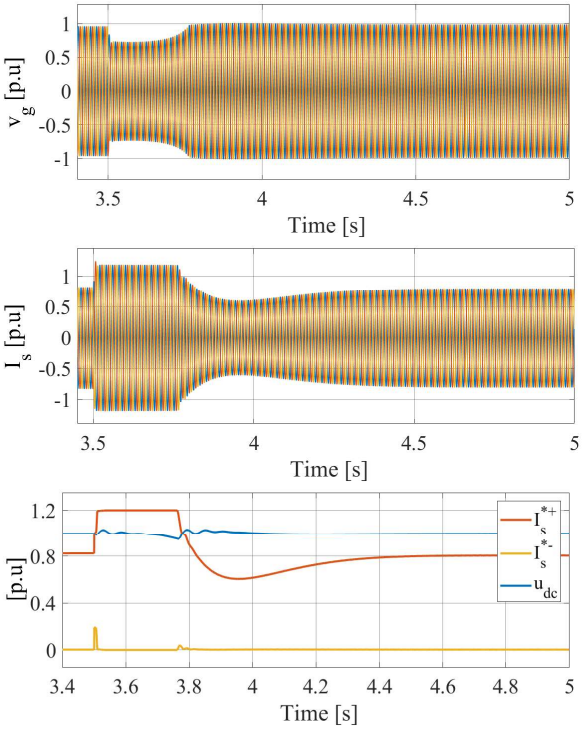

Fig. 9. Short-Circuit Ratio variation from SCR = 1.3 to SCR = 3

After 270ms, the system switched back the current control mode and stably recovered its equilibrium point within 800ms thanks to the re-synchronization function in (29).

2) Grid-connected faults at PCC: In this subsection, faults are applied in mid-line X_{g_2}, R_{g_2} and cleared by tripping the line X_{g_2}, R_{g_2} as illustrated in Fig. 10. In this test case, the inertial AC grid in Fig. 2 is considered, and a P_L of

TABLE I
SYSTEM AND CONTROL PARAMETERS

P_n	1000 MW	f_n	50 Hz
$\cos\phi$	0.95	U_e	400 kV
V_{T_2}/V_{T_1}	400/320	E_g^{+*}	1 p.u
L_c	0.15 p.u	m_p	0.04 p.u
L_{g_1}	0.76 p.u	ω_f	60 rad/s
C_f	0.066 p.u	T_1	0.2 ms
R_v	0.09 p.u	L_f	0.15 p.u
L_{g_2}	0.588 p.u	T_d	0.4s
n_q	0	T_2	0.02s
u_{dc}	640 kV	I_{max}	1.2 p.u
R_{LCL_D}	0.7 p.u	T_Q	31.4 rad/s
k_{i_v}	2.1 p.u	K_p	0.5 p.u
X/R	10	ω_R	1256 rad/s
k_p^{dc}	0.02	k_i^{dc}	0.19
C_{dc}	400 μF	T_{dc}	10ms

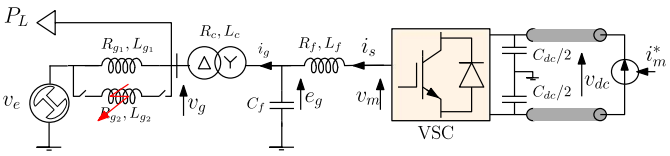

Fig. 10. Grid case for faults assessment

1000MW is connected at the PCC level and electrically close to the power converter. The aim is to evaluate the current limitation technique and the system stability under such critical circumstances: the system is switching from a strong to a very weak-grid once the fault is cleared, which engenders in addition to a voltage sag, a significant negative phase-shift of -0.436rad. The operating point of system is $P = P_g = 0.5$ p.u. Three fault scenarios listed in the following are applied at t = 3.5s 1) 250ms three-phase bolted fault, 2) 1s single-phase to ground fault, 3) 1s bi-phase fault. The results are gathered in Fig. 11, Fig. 12 and Fig. 13, respectively. The following quantities are simulated: the converter current i_s, the PCC voltage v_g, the active power, the converter current references $I_s^{\pm}$ and the DC voltage u_{dc}.

One can notice from Fig. 11 that when the three-phase fault occurs, the grid voltage at the PCC drops, which consequently yields a current rise. The latter has been well limited to its maximum allowable value $I_{max} = 1.2$ p.u. Once the fault is cleared, the system stably recovers its equilibrium point as expected within 100ms. Fig. 12 and Fig. 13 illustrate the system behavior under single-phase to ground and bi-phase faults. The results show the effectiveness of the proposed control in limiting accurately the current. During this phase, the positive sequence of the PCC voltage is about 88% for the single-phase to ground fault and 68% for the bi-phase fault, while the negative sequence is around 13% and 20%, respectively. Once the faults are cleared, the system stably recovers its equilibrium point.

IV. Conclusion

In this paper, an extended power synchronization control method has been developed and discussed. The proposed control is designed to deal with both balanced and unbalanced grid conditions. Additionally, a current limitation method has been embedded to meet the Fault Ride-Through requirements and to face large grid disturbances. To avoid the converter disconnecting after a fault, an algorithm has been adopted to enhance the transient stability and to aid for a smooth post-fault re-synchronization. The performances and the effectiveness of the proposed methods have been demonstrated through time-domain simulations. In this paper, no priority has been given to the positive sequence against the negative sequence, neither to the current d-component against the q-component. It is worthy to highlight in a future work the impact of the current limit priority on the current limitation performances and on the voltage negative sequence component.

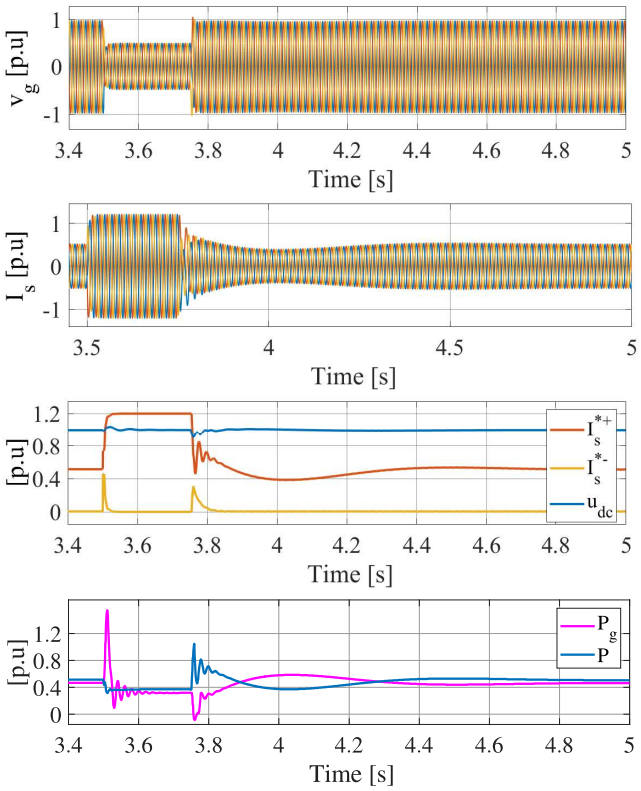

Fig. 11. VSC response to a 250ms Three-phase bolted fault

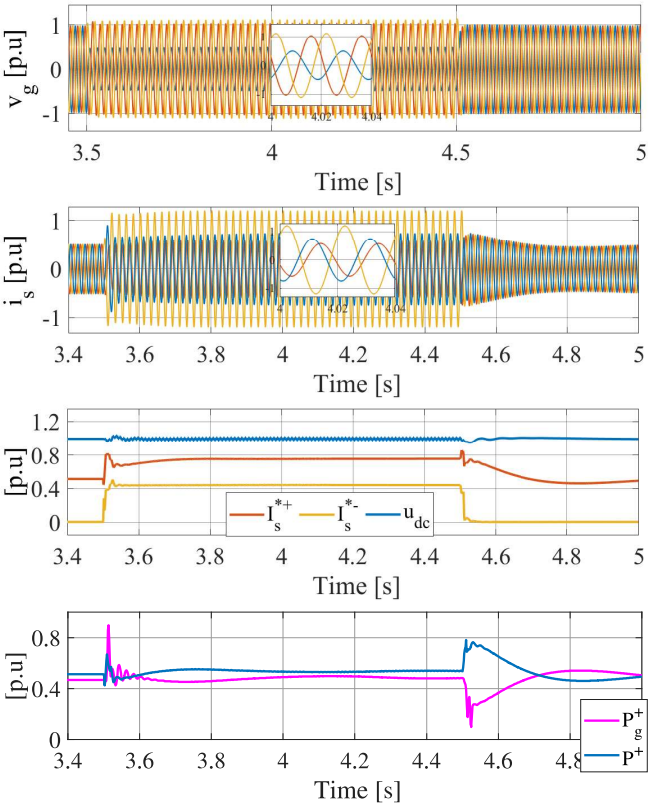

Fig. 12. VSC response to a single-phase to ground fault

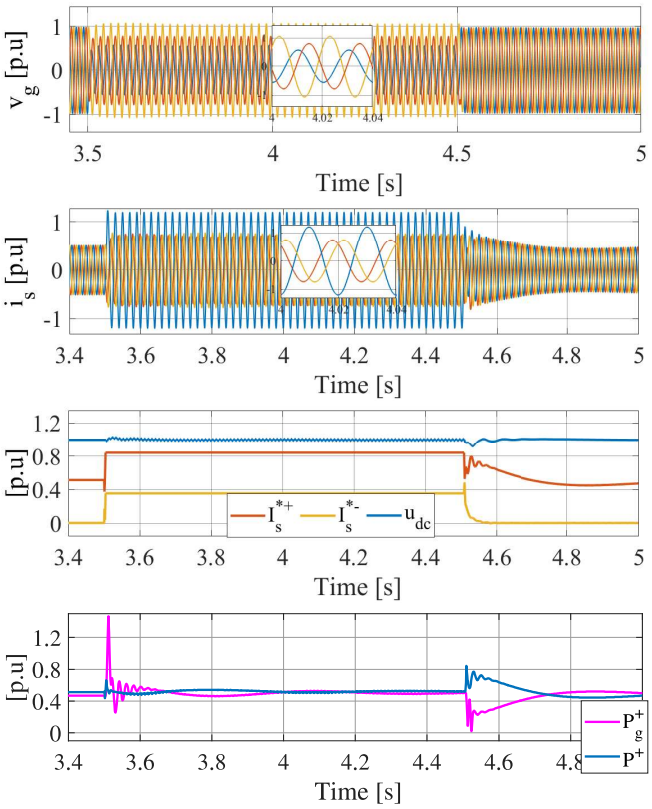

Fig. 13. VSC response to a bi-phase fault

APPENDIX

The DC voltage control is giving by the following formula:

$$i_m^* = -\left(k_p^{dc} + \frac{k_i^{dc}}{s}\right)\left(\frac{1}{1+T_{dc}s}\right)(u_{dc}^* - u_{dc}) \qquad (30)$$

REFERENCES

[1] Doğan Çelík, Mehmet Emin Meral,A flexible control strategy with overcurrent limitation in distributed generation systems, International Journal of Electrical Power & Energy Systems, Volume 104, 2019, Pages 456-471, ISSN 0142-0615, https://doi.org/10.1016/j.ijepes.2018.06.048.

[2] T. QORIA, "Grid-forming control to achieve a 100% power electronics interfaced power transmission systems," ENSAM, Paris, 2020.

[3] Doğan Çelik, Mehmet Emin Meral, A coordinated virtual impedance control scheme for three phase four leg inverters of electric vehicle to grid (V2G), Energy, Volume 246, 2022, 123354, ISSN 0360-5442, https://doi.org/10.1016/j.energy.2022.123354.

[4] S. D'Arco and J. A. Suul, "Equivalence of Virtual Synchronous Machines and Frequency-Droops for Converter-Based MicroGrids," IEEE Trans. Smart Grid, vol. 5, no. 1, pp. 394–395, Jan. 2014, doi: 10.1109/TSG.2013.2288000.

[5] J. Liu, Y. Miura, and T. Ise, "Comparison of Dynamic Characteristics Between Virtual Synchronous Generator and Droop Control in converter-Based Distributed Generators," IEEE Trans. Power Electron., vol. 31, no. 5, pp. 3600–3611, May 2016, doi: 10.1109/TPEL.2015.2465852.

[6] H. -P. Beck and R. Hesse, "Virtual synchronous machine," 2007 9th International Conference on Electrical Power Quality and Utilisation, 2007, pp. 1-6, doi: 10.1109/EPQU.2007.4424220.

[7] H2020 MIGRATE PROJECT https://www.h2020-migrate.eu/

[8] I. Sadeghkhani, M. E. Hamedani Golshan, J. M. Guerrero and A. Mehrizi-Sani, "A Current Limiting Strategy to Improve Fault Ride-Through of Inverter Interfaced Autonomous Microgrids," in IEEE Transactions on Smart Grid, vol. 8, no. 5, pp. 2138-2148, Sept. 2017, doi: 10.1109/TSG.2016.2517201.

[9] E. Rokrok, T. Qoria, A. Bruyere, B. Francois and X. Guillaud, "Transient Stability Assessment and Enhancement of Grid-Forming Converters Embedding Current Reference Saturation as Current Limiting Strategy," in IEEE Transactions on Power Systems, doi: 10.1109/TPWRS.2021.3107959

[10] M. G. Taul, X. Wang, P. Davari and F. Blaabjerg, "Current Limiting Control With Enhanced Dynamics of Grid-Forming Converters During Fault Conditions," in IEEE Journal of Emerging and Selected Topics in Power Electronics, vol. 8, no. 2, pp. 1062-1073, June 2020, doi: 10.1109/JESTPE.2019.2931477

[11] J. Freytes, J. Li, G. de Préville and M. Thouvenin, "Grid-Forming Control With Current Limitation for MMC Under Unbalanced Fault Ride-Through," in IEEE Transactions on Power Delivery, vol. 36, no. 3, pp. 1914-1916, June 2021, doi: 10.1109/TPWRD.2021.3053148

[12] A. D. Paquette and D. M. Divan, "Virtual Impedance Current Limiting for Inverters in Microgrids With Synchronous Generators," *IEEE Trans. Ind. Appl.*, vol. 51, no. 2, pp. 1630–1638, Mar. 2015.

[13] Taoufik Qoria, François Gruson, Fréderic Colas, Xavier Kestelyn, Xavier Guillaud, "Current limiting algorithms and transient stability analysis of grid-forming VSCs", Electric Power Systems Research, Volume 189, 2020, 106726, ISSN 0378-7796,

[14] X. Wang, Y. W. Li, F. Blaabjerg and P. C. Loh, "Virtual-Impedance-Based Control for Voltage-Source and Current-Source Converters," in IEEE Transactions on Power Electronics, vol. 30, no. 12, pp. 7019-7037, Dec. 2015, doi: 10.1109/TPEL.2014.2382565.

[15] Q. Taoufik, H. Wu, X. Wang and I. Colak, "Variable Virtual Impedance-based Overcurrent Protection For Grid-forming Inverters: Small-Signal, Large-Signal Analysis and Improvement," in IEEE Transactions on Smart Grid, doi: 10.1109/TSG.2022.3232987.

[16] L. Zhang, L. Harnefors and H. Nee, "Power-Synchronization Control of Grid-Connected Voltage-Source Converters," in IEEE Transactions on Power Systems, vol. 25, no. 2, pp. 809-820, May 2010, doi: 10.1109/TPWRS.2009.2032231.

[17] Zubiaga, M.; Cardozo, C.; Prevost, T.; Sanchez-Ruiz, A.; Olea, E.; Izurza, P.; Khan, S.H.; Arza, J. Enhanced TVI for Grid Forming VSC under Unbalanced Faults. Energies 2021, 14, 6168. https://doi.org/10.3390/en14196168

[18] R. Rosso, S. Engelken and M. Liserre, "On The Implementation of an FRT Strategy for Grid-Forming Converters Under Symmetrical and Asymmetrical Grid Faults," in IEEE Transactions on Industry Applications, vol. 57, no. 5, pp. 4385-4397, Sept.-Oct. 2021, doi: 10.1109/TIA.2021.3095025.

[19] N. Baeckeland, D. Venkatramanan, M. Kleemann and S. Dhople, "Stationary-Frame Grid-Forming Inverter Control Architectures for Unbalanced Fault-Current Limiting," in IEEE Transactions on Energy Conversion, vol. 37, no. 4, pp. 2813-2825, Dec. 2022, doi: 10.1109/TEC.2022.3203656.

[20] A. Meligy, T. Qoria and I. Colak, "Assessment of Sequence Extraction MethodsApplied to MMC-SDBC STATCOM Under Distorted Grid Conditions," in IEEE Transactions on Power Delivery, doi: 10.1109/TPWRD.2022.3162959

[21] Z. Shuai, C. Shen, X. Liu, Z. Li, and Z. John Shen, "Transient angle stability of virtual synchronous generators using Lyapunov's direct method," *IEEE Trans. Smart Grid*, vol. 10, no. 4, pp. 4648–4661, 2019.

[22] T. Qoria, F. Gruson, F. Colas, G. Denis, T. Prevost, and X. Guillaud, "Critical clearing time determination and enhancement of grid-forming converters embedding virtual impedance as current limitation algorithm," *IEEE J. Emerg. Sel. Top. Power Electron.*, vol. 8, no. 2, pp. 1050–1061, Jun. 2020.

[23] T. Qoria, E. Rokrok, A. Bruyere, B. Francois, and X. Guillaud, "A PLL-Free Grid-Forming Control with Decoupled Functionalities for High-Power Transmission System Applications," *IEEE Access*, vol. 8, pp. 197363–197378, Oct. 2019.

[24] X. Wang, M. G. Taul, H. Wu, Y. Liao, F. Blaabjerg and L. Harnefors, "Grid-Synchronization Stability of Converter-Based Resources—An Overview," in IEEE Open Journal of Industry Applications, vol. 1, pp. 115-134, 2020, doi: 10.1109/OJIA.2020.302039

[25] D. Pan, X. Wang, F. Liu, and R. Shi, "Transient Stability Impact of Reactive Power Control on Grid-Connected Converters," in Proc. IEEE Energy Conversion Congress and Exposition (ECCE), Baltimore, MD, USA, 2019, pp. 4311–4316.

[26] T. Qoria, F. Gruson, F. Colas, G. Denis, T. Prevost and X. Guillaud, "Inertia effect and load sharing capability of grid forming converters connected to a transmission grid," 15th IET International Conference on AC and DC Power Transmission (ACDC 2019), 2019, pp. 1-6, doi: 10.1049/cp.2019.0079.